Supporting Information

A dynamic solid oxide fuel cell empowered by the

built-in iron-bed solid-fuel

Cuijuan Zhang[a], Chengxiang Ji[b], Wensheng Wang[b], Doug Schmidt[b], Xinfang Jin[a],

John P. Lemmon[c], and Kevin Huang[a*]

[a]Department of Mechanical Engineering, University of South Carolina, Columbia, SC 29208.

[b]Atrex Energy, 19 Walpole Park South, Walpole, MA 02081-2531.

[c]Advanced Research Project Agency – Energy, US Department of Energy. Present address:

National Institute of Clean and Low-carbon Energy, Beijing, China

The supporting information includes:

Section S1: Nernst potential calculation

Section S2: Theoretical finite element analysis

Section S3: Scaling power ramping rate from single cell to MW system

Section S4: Power consumed by the pump in the H_2/H_2O channel

Section S5: Fe-bed derived H_2 *vs* tanked H_2: a cost comparison

Section S6: References

Section S1: Nernst potential calculation

For an SOFC with the iron bed and 97% H_2-H_2O as the starting fuel, the reaction of $Fe + H_2O\ (g) = FeO + H_2(g)$ take places as long as $U_f \geq 30.8\%$ (at 750 °C). Under such a circumstance, the total reaction changes from conventional $2H_2 + O_2 = 2H_2O$ to

$$2Fe + O_2 = 2FeO \qquad\qquad (S1)$$

after combining with the following simultaneous reaction inside the iron bed

$$H_2O + Fe = FeO + H_2 \qquad\qquad (S2)$$

The cell Nernst potential E_N is 0.989 V *vs.* air at 750 °C for the reaction (S1) according to the following Nernst equation:

$$E_N = \frac{RT}{4F} ln\left(\frac{0.21}{\frac{1}{K}}\right) \qquad\qquad (S3)$$

where K is the equilibrium constant of reaction $2Fe + O_2 = 2FeO$ at temperature of T; T is the temperature in K, 1023.15 K for this study; R is the gas constant, 8.314 J mol^{-1} K^{-1}; F is the Faraday constant, 96485 C mol^{-1}; 0.21 is the molar fraction of oxygen in air.
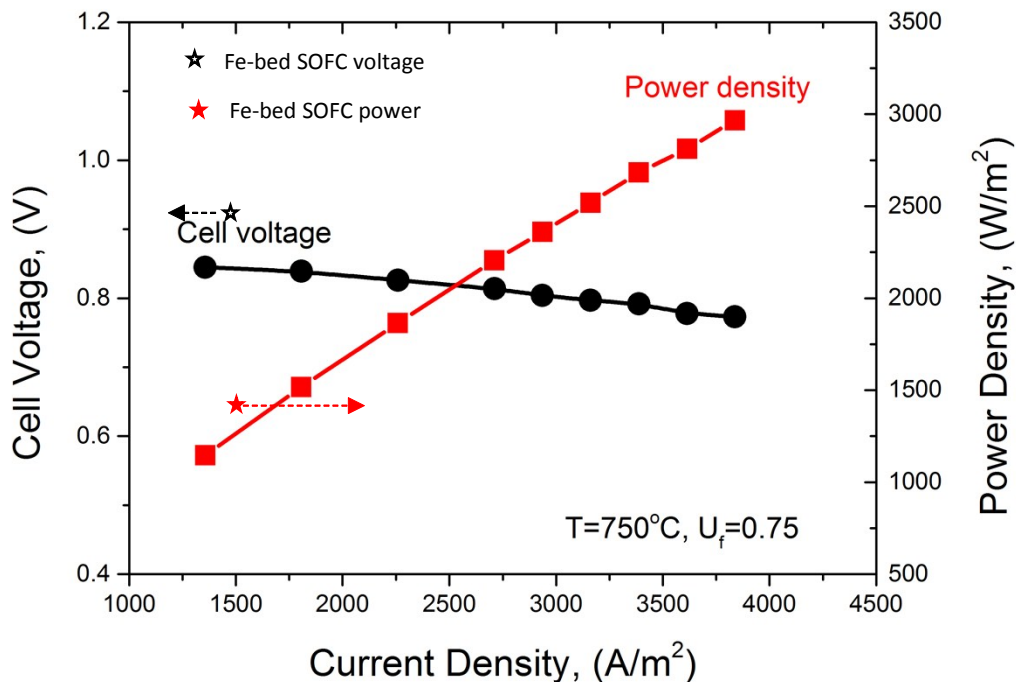
Fig. S1. I-V and I-P curve for the Fe-bed-free SOFC at 750 °C with $H_2/3\%H_2O$ as fuel and air as oxidant. For the Fe-bed loaded case, the current, voltage and power at U_f of 75% is included.

The I-V curve is typical for the pilot-scale SOFC. We did not measure the I-V curve of the Fe-bed-loaded SOFC. The I-V curve is expected to be similar with the Fe-bed-free case except that its voltage is higher due to extra hydrogen generated. We only marked cell voltage and power of Fe-bed SOFC in Fig. S1 at 150 mA/cm^2 from our overload testing.

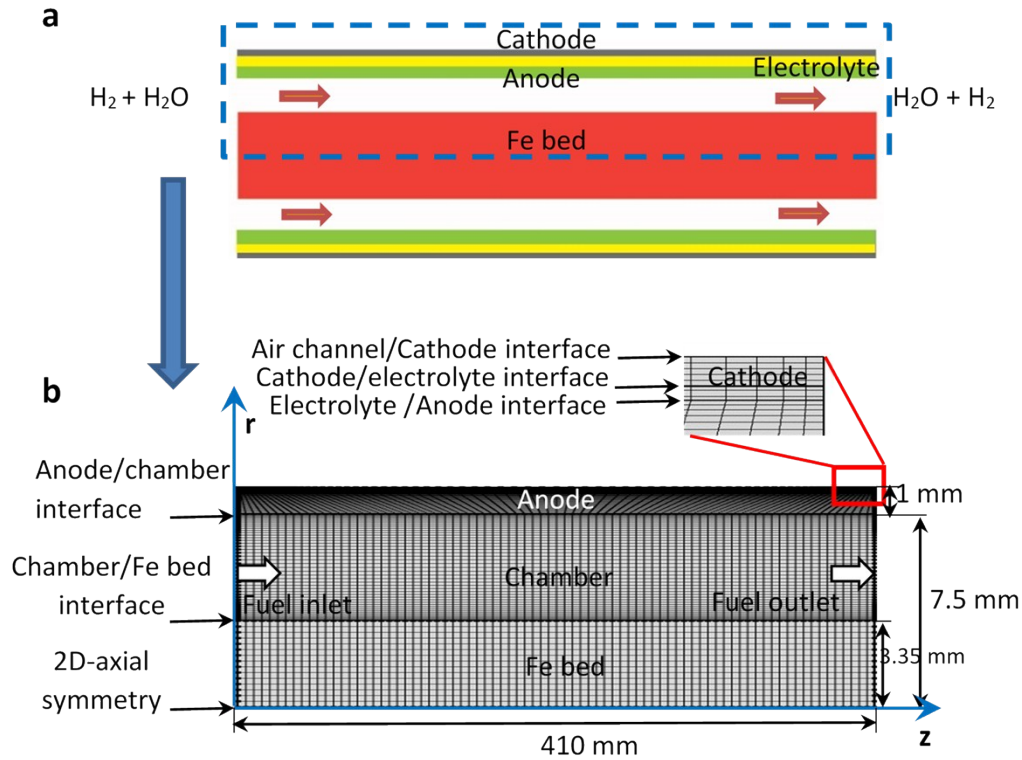## Section S2: Theoretical finite element analysis

Fig. S2 Model used for theoretical finite-element analysis. a Cross-sectional view of the anode-supported tubular SOFC. b 2D axial symmetric computational domains and boundaries.

There are a total of 8 dependent variables in the model, including the electronic potential ϕ_e and ionic potential ϕ_i, mass fraction of the gas species, ω_j ($\omega_1, \omega_2, \omega_3$ in the O_2 electrode, ω_4 and ω_5 in the H_2 electrode, chamber and Fe bed), and the reacted fraction ratio x_{Fe}. By combining governing equations in Table S1-2 with the boundary conditions in Table S3 and the initial conditions, those variables are solved simultaneously as a function of time and positions.

Table S1 Governing equations and variables

Domain	Governing equation	Dependent variable
SOFC cathode pores	$$\frac{\partial(\varepsilon\rho\omega_i)}{\partial t}+\nabla\cdot\left(-\rho\omega_i\sum_{j=1}^{3}D_{ij}^{eff}\left(\frac{M}{M_j}\left(\nabla\omega_j+\omega_j\frac{\nabla M}{M}\right)\right)\right)=R_i,(i=1,2)$$ $$\omega_3=1-\sum_{i=1}^{2}\omega_i\quad M=\left(\sum_{i=1,2,3}\frac{\omega_i}{M_i}\right)^{-1}$$	$\omega_1,\omega_2,\omega_3$
SOFC cathode solid phase	$$\begin{cases}\nabla\cdot\left(-\sigma_{e,o}\nabla\phi_e\right)=+S_{a,o}i_{ict,o}\\ \nabla\cdot\left(-\sigma_{i,o}\nabla\phi_i\right)=-S_{a,o}i_{ict,o}\end{cases}$$	ϕ_e, ϕ_i
Electrolyte	$$\nabla\cdot\left(-\sigma_{i,el}\nabla\phi_i\right)=0$$	ϕ_i
SOFC anode solid phase	$$\begin{cases}\nabla\cdot\left(-\sigma_{e,h}\nabla\phi_e\right)=-S_{a,h}i_{ict,h}\\ \nabla\cdot\left(-\sigma_{i,h}\nabla\phi_i\right)=+S_{a,h}i_{ict,h}\end{cases}$$	ϕ_e, ϕ_i
SOFC anode pores	$$\frac{\partial(\varepsilon\rho\omega_i)}{\partial t}+\nabla\cdot\left(-\rho\omega_i\sum_{j=4}^{5}D_{ij}^{eff}\left(\frac{M}{M_j}\left(\nabla\omega_j+\omega_j\frac{\nabla M}{M}\right)\right)\right)=R_i,(i=4)$$ $$\omega_5=1-\omega_4\quad M=\left(\sum_{i=4,5}\frac{\omega_i}{M_i}\right)^{-1}$$	ω_4,ω_5
Chamber	$$\frac{\partial(\rho\omega_i)}{\partial t}+\nabla\cdot\left(-\rho\omega_i\sum_{j=4}^{5}D_{ij}\left(\frac{M}{M_j}\left(\nabla\omega_j+\omega_j\frac{\nabla M}{M}\right)\right)\right)+\rho\left(\mathbf{u_0}\cdot\nabla\omega_i\right)=R_i,(i=4)$$ $$\omega_5=1-\omega_4\quad M=\left(\sum_{i=4,5}\frac{\omega_i}{M_i}\right)^{-1}$$	$,\omega_5$
Fe bed-Pores	$$\frac{\partial(\varepsilon\rho\omega_i)}{\partial t}+\nabla\cdot\left(-\rho\omega_i\sum_{j=4}^{5}D_{ij}^{eff}\left(\frac{M}{M_j}\left(\nabla\omega_j+\omega_j\frac{\nabla M}{M}\right)\right)\right)=R_i,(i=4)$$ $$\omega_5=1-\omega_4\quad M=\left(\sum_{i=4,5}\frac{\omega_i}{M_i}\right)^{-1}$$	ω_4,ω_5
Fe bed-solid phase	$$\frac{dx_{Fe}}{dt}=\left(k_{f,J}x_{H_2O}-k_{b,J}x_{H_2}\right)N\left(1-x_{Fe}\right)\left[-\ln(1-x_{Fe})\right]^{\frac{N-1}{N}}$$	x_{Fe}

Table S2 Associated source terms and variables used in the model

Source terms /variables	Mathematical expressions
Butler-Volmer equation	$$i_{ict,o}=i_0\left(\exp\left(\frac{\alpha_1 F}{RT}\eta_o\right)-\frac{c_{O_2}}{c_{O_2}^0}\exp\left(-\frac{\alpha_2 F}{RT}\eta_o\right)\right)$$

$$i_{ict,h} = i_0 \left(\frac{c_{H_2}}{c_{H_2}^0} \exp\left(\frac{\alpha_1 F}{RT} \eta_h \right) - \frac{c_{H_2O}}{c_{H_2O}^0} \exp\left(-\frac{\alpha_2 F}{RT} \eta_h \right) \right)$$

$$\eta_{o/h} = \phi_e - \phi_i - \Delta\phi_{eq,o/h}, \quad \Delta\phi_{eq,h} = 0V$$

$$\Delta\phi_{eq,o} = E^0 - \frac{RT}{2F} ln\left(\frac{p_{H_2O,h}}{p_{O_2,o}^{0.5} \, p_{H_2,h}} \right), \quad E^0 = 0.992V$$

Binary diffusion	$D_{ij} = k_D \dfrac{T^{1.75}}{p\left(v_i^{1/3} + v_j^{1/3}\right)^2} \left[\dfrac{1}{M_i} + \dfrac{1}{M_j} \right]^{1/2}$
Knudsen diffusion	$D_{Kn,i} = \dfrac{97}{2} d_{pore} \sqrt{T/M_i}$, $\quad d_{pore} = \dfrac{2}{3} \dfrac{\varepsilon d_p}{1-\varepsilon}$
Average Bosanquet diffusion coefficient	$D_{ij}^{eff} = \dfrac{1}{2} \dfrac{\varepsilon}{\tau} \left(\dfrac{1}{\dfrac{1}{D_{ij}} + \dfrac{1}{D_{Kn,i}}} + \dfrac{1}{\dfrac{1}{D_{ij}} + \dfrac{1}{D_{Kn,j}}} \right)$
Source term	$R_{O_2,o} = -\dfrac{i_{ict,o} S_{a,o} M_{O_2}}{4F}$, $R_{H_2,h} = -\dfrac{i_{ict,h} S_{a,h} M_{H_2}}{2F}$, $R_{H_2O,h} = \dfrac{i_{ict,h} S_{a,h} M_{H_2O}}{2F}$ $R_{H_2,bed} = \dfrac{dx_{Fe}}{dt} c_{Fe}\left(1-\varepsilon_{bed}\right)M_{H_2}$, $R_{H_2O,bed} = -\dfrac{dx_{Fe}}{dt} c_{Fe}\left(1-\varepsilon_{bed}\right)M_{H_2O}$
Reaction equilibrium constant for Fe bed	$K = \exp\left(-\dfrac{\Delta G^0}{RT} \right) = \dfrac{x_{H_2}}{x_{H_2O}} = \dfrac{k_f}{k_b} = 2.05$, under 750°C(Eq. S3)
Fe bed Porosity	$\varepsilon_{bed} = \varepsilon_0 + \left(1-\varepsilon_0\right)x_{Fe}c_{Fe}\left(\dfrac{M_{Fe}}{\rho_{Fe}} - \dfrac{M_{FeO}}{\rho_{FeO}} \right)$

Table S3 Boundary conditions used in the model

Boundary	Electronic potential	Ionic potential	Stefan-Maxwell diffusion
Dependent Variable	ϕ_e	ϕ_i	ω_j
Air channel/cathode	Cell voltage	$-\underline{n} \cdot \nabla\phi_i = 0$	O_2:N_2:H_2O=0.238:0.742:0.02
Cathode/electrolyte interface	$-\underline{n} \cdot \nabla\phi_e = 0$	Continuity	$-\underline{n} \cdot \underline{N_i} = 0$
Electrolyte/anode interface	$-\underline{n} \cdot \nabla\phi_e = 0$	Continuity	$-\underline{n} \cdot \underline{N_i} = 0$
Anode/Chamber	0 V	$-\underline{n} \cdot \nabla\phi_i = 0$	Continuity
Chamber inlet	N/A	N/A	H_2:H_2O = 0.79:0.21
Chamber outlet	N/A	N/A	$-\underline{n} \cdot \rho\omega_i \sum_j D_{ij}^{eff} \underline{d}_j = 0$
Chamber/Fe bed	N/A	N/A	Continuity

Other surfaces	$-\underline{n} \cdot \nabla \phi_e = 0$	$-\underline{n} \cdot \nabla \phi_i = 0$	$-\underline{n} \cdot \underline{N}_i = 0$

Note: $\underline{N_i} = -\rho \omega_i \sum_j D_{ij}^{eff} \underline{d_j} + \rho u \omega_i$, $\underline{d_j} = \left(\frac{M}{M_j} \left(\nabla \omega_j + \omega_j \frac{\nabla M}{M} \right) \right)$.

To ensure high fidelity of the model, the parameters of the SOFC were extracted from an experimental V-I curve, as shown in Fig. S3. Note that Fig. S3 is the same as Fig. S1 in terms of experimental data. The reaction rate constants of the JMAK model were referred to in our previous model validated by an 800 °C button cell loaded with a Fe bed [1] with the equilibrium constant modified for an operating temperature at 750 °C. The parameters are listed in Table S4.
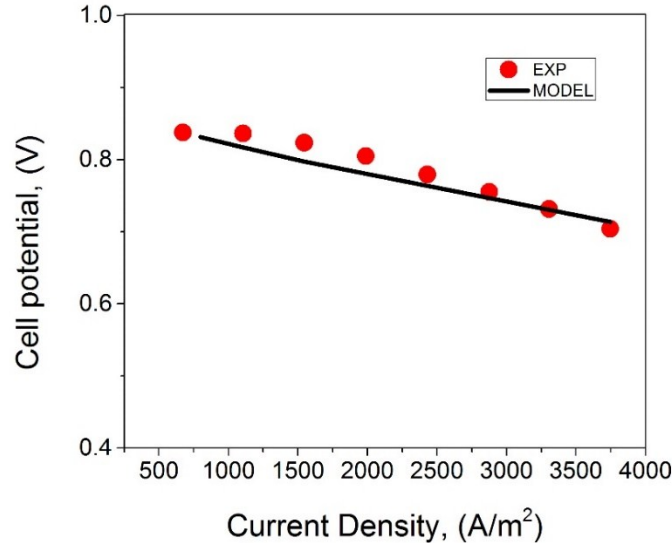

Fig. S3 Comparison of experimental and modelling results. Validation of exchange current density from a V-I curve obtained from a tubular SOFC without Fe bed at 750 °C.

Table S4 Parameters used in the model

Parameters	750 °C Fe-bed cell
Atmospheric pressure, p_0 (atm)	1
Temperature, T_0 (°C)	750
Inlet mass fraction of H_2 $x_{ref,H2}$	0.79
Inlet mass fraction of O_2 $x_{ref,O2}$	0.238
Porosity, Anode/Cathode ε	0.55/0.55

Electronic conductivity, σ_e (S m^{-1})	5×10^6
Ionic conductivity, $\sigma_{i,el}$* (S m^{-1})	1.92
Exchange current density for SOFC, Anode/Cathode i_0* (A m^{-2})	1064/3990
Specific surface area, Anode/Cathode S_a* (m^{-1})	$(1-\varepsilon_{a/c}) \times 1.43 \times 10^5$
Transfer coefficient, α_1/ α_2	0.5/1.5
Number of electrons, n	2
Reference diffusivity, k_D (m^2 s^{-1})	3.16×10^{-8}
Kinetic volume of H_2, vh_2	6×10^{-6}
Kinetic volume of O_2, vo_2	16.6×10^{-6}
Kinetic volume of N_2, vn_2	17.9×10^{-6}
Kinetic volume of H_2O, vh_2o	12.7×10^{-6}
Diameter of spherical particle, Anode/Cathode, d_p (μm)	0.5
Loading of Iron, m_{Fe} (g)	34.16
Initial reacted Fe ratio, $x_{Fe,0}$	10^{-4}
Initial porosity of RCU, ε	0.7
Reaction rate constant of JMAK, $k_{f,J}/k_{b,J}$ (s^{-1})	$9.4 \times 10^{-4}/4.585 \times 10^{-4}$
Avrami exponent of JMAK, N	0.8
Flow velocity in the Chamber, u_0, (m s^{-1})	0.138

Note: The parameters with * are adjusted in order to validate the model with the experimental results.

Nomenclature used in the model

c (mol m^{-3})	Molar concentration
d_{pore} (m)	Diameter of spherical particle of the porous medium
d_p (m)	Pore radius of the porous medium
D_{ij} (m^2 s^{-1})	Binary diffusion coefficient for a pair of species i and j
D_{kn},i (m^2 s^{-1})	Knudsen diffusion coefficient of species i
E (V)	Nernst potential
F (C mol^{-1})	Faraday's constant, 96485
G (J mol^{-1})	Gibbs free energy
i_{ict} (A m^{-2})	Local charge transfer current density
K	Equilibrium constant
k_D (m^2 s^{-1})	Reference diffusivity
k_{fJ} (s^{-1})	Forward reaction constant in JMAK model
k_{bJ} (s^{-1})	Backward reaction constant in JMAK model
M_i (kg mol^{-1})	Molar weight of species i
M (kg mol^{-1})	Average molar weight of gas mixture
N	Avrami exponent
p (Pa)	Pressure

R (J mol^{-1} K^{-1}))	Gas constant, 8.314
R$_i$ (kg m^{-3} s^{-1})	Reaction source term for species i
Sa (m^{-1})	Electrochemical reaction active area per unit volume
T (K)	Temperature
t (s)	Time
x$_{Fe}$	Reacted Fe ratio

Greek symbols

α	Transfer coefficient in Butler-Volmer equation
σ	Conductivity, (S·m^{-1})
ϕ (V)	Potential
$\Delta\phi_{eq}$ (V)	Equilibrium potential
H (V)	Overpotential
ρ (kg m^{-3})	Density
$\omega_{i/j}$	Mass fraction of species i/j
v_i	Kinetic volume of species i
ε	Porosity
τ	Tortuosity

Subscripts

e	Electronic
el	Electrolyte
i	Ionic
o	Oxygen electrode
h	Hydrogen electrode

Superscripts

| eff | Effective |
| **0** | Ideal/Initial |

Section S3: Scaling power ramping rate from single cell to MW system

To show the potential of the Fe-bed SOFC technology as a dynamic power generator for large scale utility grid stabilization applications, we performed a simple scaling calculation from the single cell performance presented in the main context to a 1 MW system. The basis for the scaling is that a single Atrex SOFC produces 30 W. Since each cell can provide a ramping power rate of 11 W cm^{-2} min^{-1} (or ~2.5 kW min^{-1} per cell) the total ramping power capacity for a 1 MW baseload SOFC generator will be 10^6 W/30 W $\times$ 11 W cm^{-2} min^{-1} $\times$ 80% = 0.33 MW cm^{-2} min^{-1}, by assuming a 20% power loss during scaling from single cell to stack. From a total power point of view, 0.33 MW cm^{-2} min^{-1} is equivalent to 67 MW min^{-1} for a 1 MW SOFC generator system.

Section S4: Pressure drop calculations in the Fe-bed loaded fuel channel

One concern over the Fe-bed-loaded SOFC is whether the Fe-bed solid fuel would increase the pressure drop of fuel in the fuel channel, which in turn increases the parasitic fuel-pump power consumption. Therefore, we performed a fuel pressure-drop analysis across the fuel channel and the corresponding fuel-pump power consumption. The computational domains and corresponding velocity distributions in the tubular SOFC with and without the Fe bed are illustrated in Figure S6. The multicomponent H_2/H_2O transport in all the domains is governed by Maxwell-Stefan's diffusion and convection equation. We used the Navier-Stokes equations to describe the weakly compressible flow of H_2/H_2O in the fuel channels and the Brinkman equations to describe the flow velocity in the porous anode and Fe-bed.

From the computed results, it shows that to achieve a 0.315 slpm inlet fuel flow (corresponding to the total current 33.89A and fuel utilization 75%), the pressure drop between the inlet and outlet is 0.2 Pa for an Fe-bed-free fuel channel shown in Fig. S4 a and 1.2 Pa for an Fe-bed loaded fuel channel as shown in Fig. S4 b. The mass flow rate corrected for the operating temperature at 750 °C is:

$$flow = 0.315 \, (slpm) \times \frac{1}{1000 \, (l \, m^{-3}) \times 60 (s \, min^{-1})} \times \frac{(750 + 273.15)(K)}{273.15 \, (K)} = 2.16 \times 10 \quad m^3 \, s^{-1})$$

(S4)

The pumping power can then be calculated by:

$$Power = \Delta p \times flow \tag{S5}$$

For the Fe-bed-free fuel channel, the additional fuel-pump power consumption is

$$Power = 0.2 \, (Pa) \times 2.16 \times 10^{-5} (m^3 \, s^{-1}) = 4.32 \times 10^{-6} \, (W) \tag{S6}$$

Whereas for the Fe-bed loaded fuel channel, it is

$$Power = 1.2\ (Pa) \times 2.16 \times 10^{-5}(m^3 s^{-1}) = 2.59 \times 10^{-5}\ (W) \tag{S7}$$

In comparison to the power generated by the fuel cell (assuming a working voltage of 0.9 V):

$$Power = 0.9\ (V) \times 33.89(A) = 30.5\ (W) \tag{S8}$$

The additional power consumption of the fuel-pump by the presence of the Fe-bed solid fuel in fuel channel is negligible.
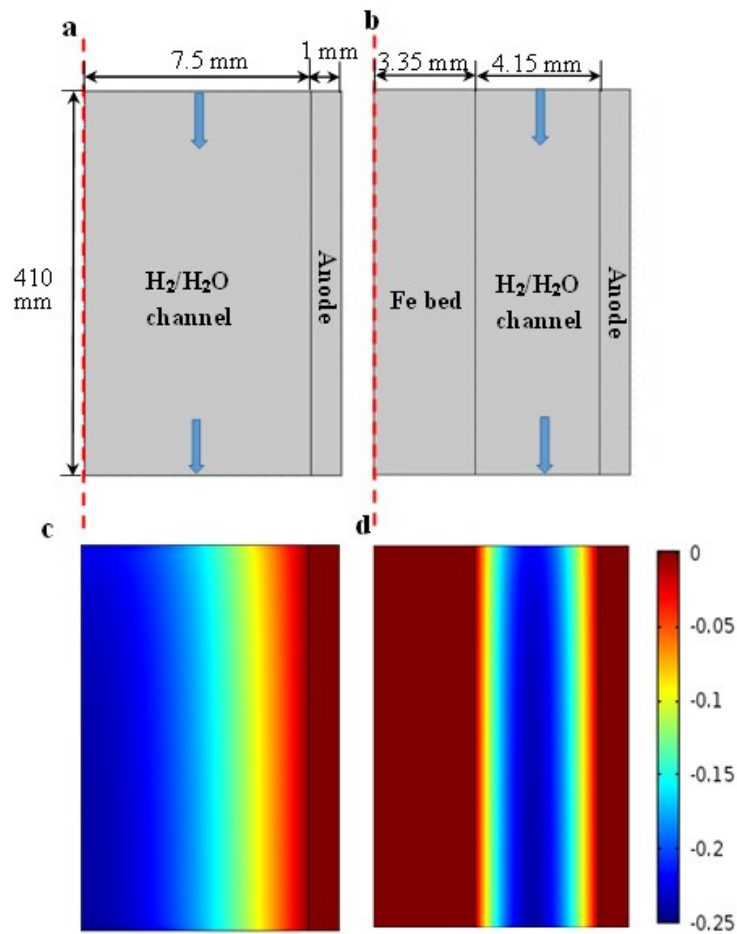

Fig. S4 Computational domains and corresponding velocity distributions inside of fuel channel. a, c without Fe-bed. b, d with Fe-bed.
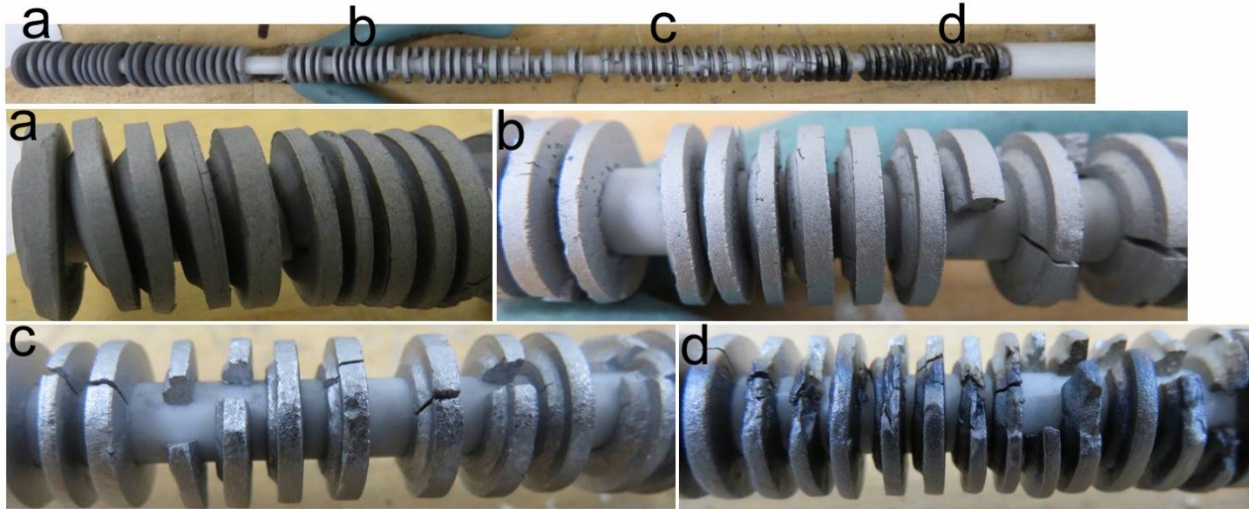
Fig. S5. Digital photographs of the appearances of the Fe-bed along axial locations after test. (a) At the close end of the tubular SOFC and (d) at the open end.
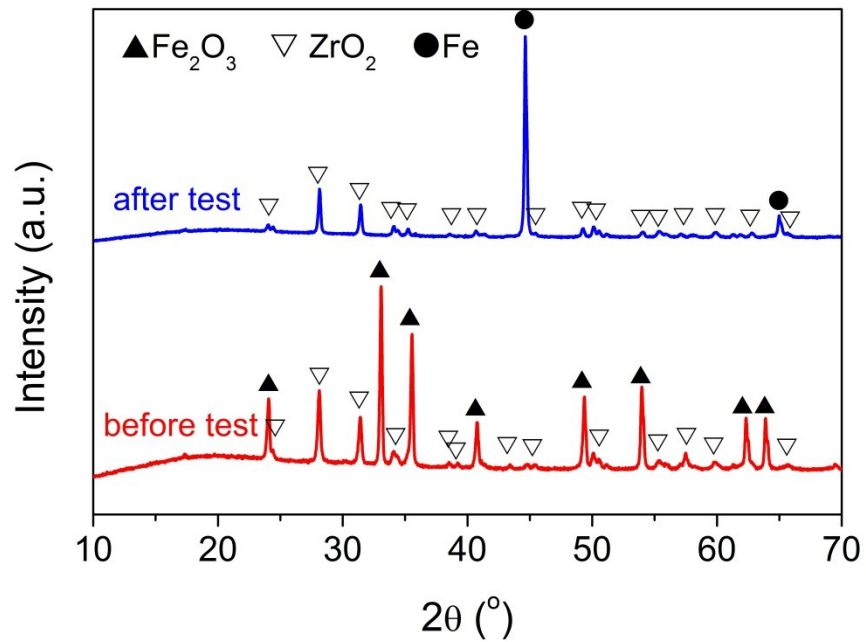

Fig. S6 XRD patterns of the Fe-bed before and after test showing no compositional change in the bulk of Fe-bed material
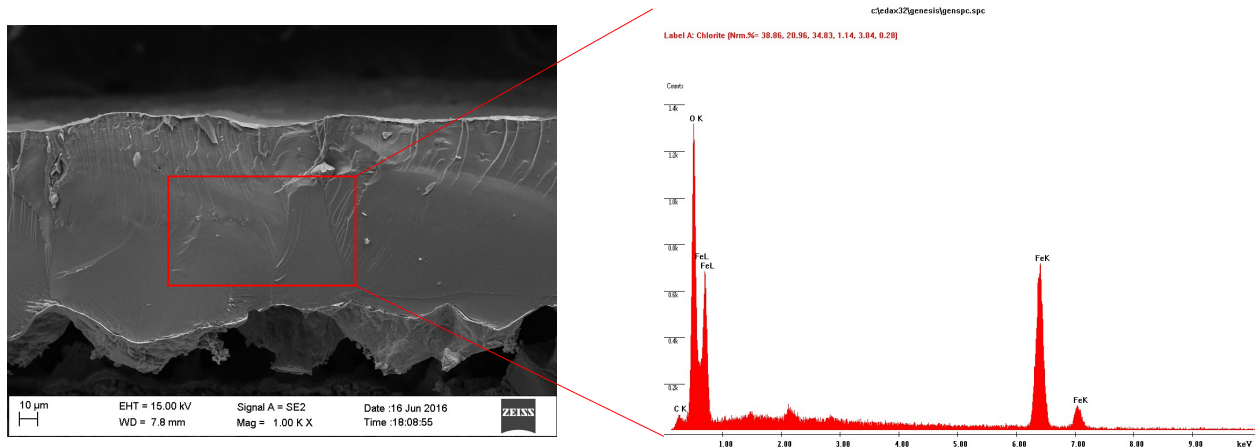
Fig. S7 EDS analysis of the dense FeO scale showing a Fe-enriched composition for the Fe-bed at the open end.

Section S5: Iron-bed H$_2$ *vs* tanked H$_2$: a cost comparison

We acknowledge that tanked H$_2$ is needed for Fe-bed SOFC due to the reason of Ni-anode and Fe-bed conditioning during the start-up. The best value of the Fe-bed is its ability to provide fast H$_2$ for overload and load-following operation, which tanked H$_2$ cannot do. Economically, Fe-bed H$_2$ is also attractive. We performed the following cost estimate solely for the purpose of comparison.

The price of iron metal is \$57.4 ton^{-1} [2] while it is \$31.97/261ft^3 for tanked H$_2$ (99.995%) [3]. From the density of iron 7.86 g cm^{-3} and hydrogen gas 0.0056 lb ft^{-3} at STP (0 °C and 1 atm), it can be calculated that producing 1 mole H$_2$ from iron only costs \$0.0032 with 7.105 cm^3 occupying volume. In contrast, the commercial H$_2$ tank would cost \$0.1 for 1 mole H$_2$ with a tank volume of 165 cm^3 at 2000 psi.

To sustain a power of 67.1 W at a current of 100.0 A, the cell without an iron bed needs a flow of 0.928 slpm H$_2$ to achieve U$_f$ = 75%. The extra hydrogen (0.928 - 0.315 = 0.613 slpm) needed means an extra cost of \$0.0026 min^{-1} and extra volume of 4.5 cm^3 H$_2$ (at 2000 psi) per min if a tanked H$_2$ is used. In contrast, it only costs \$0.000088 min^{-1} and 0.19 cm^3 Fe min^{-1} if a solid iron bed is used as the solid fuel for H$_2$ conversion; this estimate represents two orders of magnitude cheaper and 20× smaller volume than tanked H$_2$.

Section S6: References

1   X. Jin, A. M. Uddin, X. Zhao, R. White and K. Huang, *J. Electrochem. Soc.,* 2015, **162**, A1476.
2   https://www.quandl.com/collections/markets/industrial-metals.
3   www.praxair.com.